



Original Article

A New and Safe Spirocyclic Alkoxy Phosphazene: Synthesis, Characterization, DFT, Molecular Docking and Photophysical Properties

Camelia Gholamrezazadeh^{id}, Mohammad Hakimi*^{id}, Mehdi Dadmehr^{id}

Chemistry Department, Payam Noor University, Tehran, Iran

ARTICLE INFO

Article history

Submitted: 2023-09-28

Revised: 2023-11-16

Accepted: 2023-11-24

Manuscript ID: CHEMM-2310-1735

Checked for Plagiarism: Yes

Language Editor:

Dr. Fatimah Ramezani

Editor who approved publication:

Dr. Abdolkarim Zare

DOI:10.48309/chemm.2023.422145.1735

KEYWORDS

Antibacterial

MTT assay

DFT

Chemo sensor

Spirocyclic phosphazene

Molecular Docking

ABSTRACT

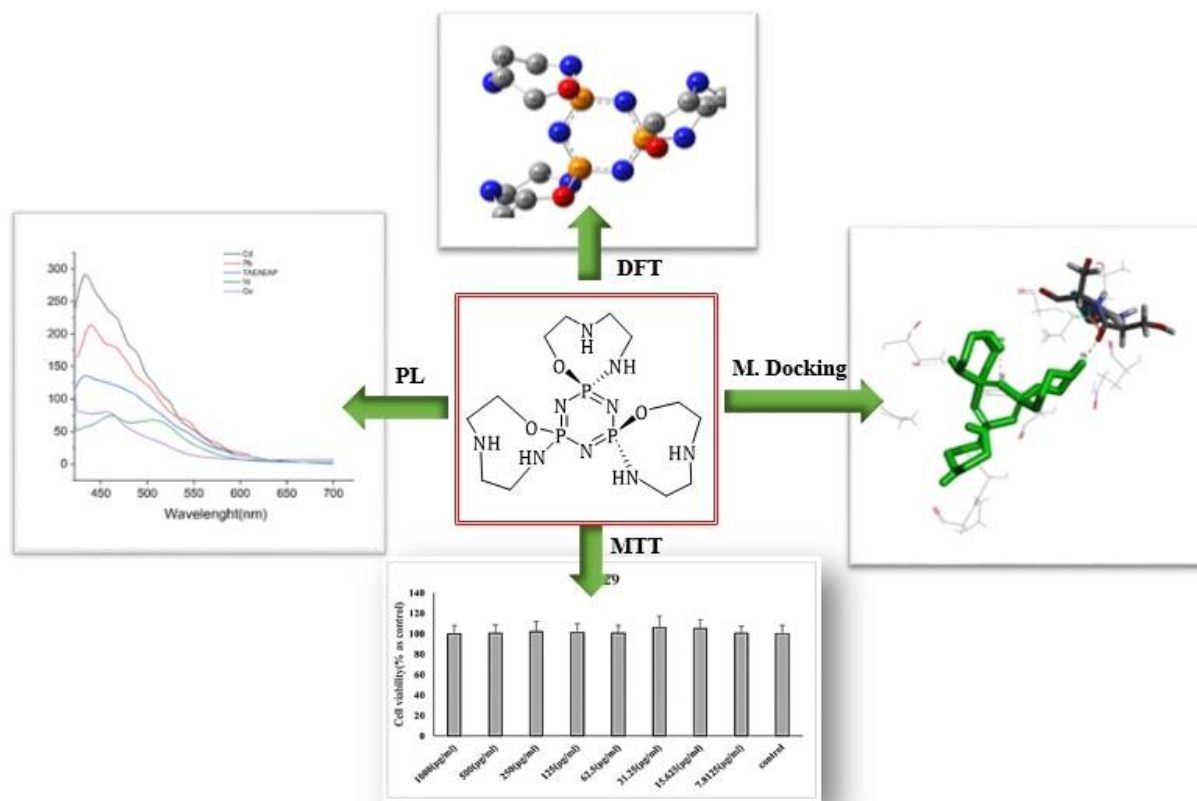
An eight-membered spiro-alkoxy compound Tris[*N*-(2-(λ^1 -oxidanyl(ethyl)-2-(λ^2 -azanyl) ethan-1-amine) $N_3P_3(OC_2H_5NC_2H_5N)_3$ was synthesized by replacing the chlorine atoms of Hexachlorocyclotriphosphazene (HCCTP) with 2-[(2-aminoethyl)amino]ethanol (AEAE) groups. The structure of Tris[*N*-(2-(λ^1 -oxidanyl(ethyl)-2-(λ^2 -azanyl) ethan-1-amine) (TAEAEAP), was characterized through the utilization of several spectroscopic techniques, such as IR, 1H -NMR, ^{13}C -NMR, ^{31}P -NMR, UV, and fluorescence spectroscopy. In addition, we performed DFT level for predicting vibrational spectra, to obtain structural parameters, including the conformation of the substitutional rings, bond lengths, and bond angles. The theoretical and experimental vibrational spectra were compared to validate the proposed model. Moreover, we investigated the emission spectra of TAEAEAP in the presence and absence of metal cations, such as Pb^{2+} , Cu^{2+} , Ni^{2+} , and Cd^{2+} , in a safe and non-toxic solvent mixture of $H_2O/MeOH$ (9:1, v/v). The biocompatibility of TAEAEAP was evaluated through an MTT assay conducted on healthy L929 fibroblast cells. Furthermore, molecular docking studies of TAEAEAP with tumour suppressor (1BD8) and transferase/transferase inhibitor (3NUP) proteins were performed. This study involved an investigation into the synthesis, structural analysis, and antibacterial properties of a purple-coloured complex, bis[tris(2-ethylaminoethyl)amine]copper(II) dinitrate, that was formed from the reaction between copper nitrate and TAEAEAP.

* Corresponding author: Mohammad Hakimi

✉ E-mail: m.hakimi@pnu.ac.ir

© 2023 by SPC (Sami Publishing Company)

GRAPHICAL ABSTRACT



Introduction

Amino alcohols, like 2-[(2-aminoethyl)amino]ethanol [1,2], are important in substitution reactions because they can act as both nucleophiles and leaving groups. In alkoxy phosphazene chemistry, this type of ligand can help create a range of structural motifs through its involvement in substitution reactions. It can donate its amino group as a nucleophile and also serve as a leaving group during the reaction, allowing for the formation of different substituted products with diverse structural properties [3-6]. When subjected to a reaction with hexachlorocyclotriphosphazene, this ligand exhibits a pronounced inclination toward the formation of spiro products [7,8]. This transformation entails the nucleophilic deprotonation of the amino group, leading to the displacement of two chlorine atoms on the same phosphorus atom of the phosphazene trimer by hydroxyl groups [9]. The size and geometry of the appended rings in the resultant cyclotriphosphazene structure are contingent

upon the length of the difunctional nucleophilic reagents employed.

The family of substituted cyclotriphosphazenes holds a prominent position in the realm of inorganic heterocyclic systems, offering a versatile array of applications, encompassing drug delivery systems [10], lubricant [11,12], flame retardant [13-15], chemo-sensors [16-18], and anticancer agents [19-21]. Hexachlorocyclotriphosphazene ($N_3P_3Cl_6$) is a cyclic compound, can be used to make various types of polymers with special properties [22]. Some of these polymers are useful for making fire-resistant [22], biocompatible, and optoelectronic materials [22]. Hexachlorocyclotriphosphazene also has other applications, such as sterilization, fertilization, and cancer treatment. In the context of this study, we successfully synthesized a fully substituted phosphazene compound with twisted octahedral rings through a solvothermal reaction.

Specifically, 2-[(2-aminoethyl)amino]ethanol (AEAE) was reacted with hexachlorocyclotriphosphazene (HCCTP) in the presence of triethylamine at a temperature of

70 °C using anhydrous toluene as the solvent for a duration of 9 days. The ratio of HCCTP to AEAE utilized in the reaction was 1:6. The structural characterization of this compound was accomplished through a comprehensive analysis employing ^1H , ^{13}C , and ^{31}P -NMR spectroscopy, complemented by IR spectroscopy. Furthermore, the spectral features related to light absorption were examined via fluorescence and ultraviolet spectroscopy.

To gain insights into the spatial geometry, symmetry, bond lengths, and angles within the synthesized compound's liquid state, we conducted density-functional theory (DFT) optimization and frequency calculations at the M06-2x/6-31G level. Comparison was made between the experimental IR spectrum and the IR spectrum obtained through computational simulations. In addition, the compound's photoelectron properties were probed in the context of its potential role as a chemo-sensor for Pb^{2+} , Cd^{2+} , Cu^{2+} , and Ni^{2+} ions in a solvent mixture of water and alcohol (methanol) at a ratio of 1:9 (v/v), a configuration that capitalizes on the notable fluorescence characteristics of the spiroalkoxy compound in DMSO solvent.

The biocompatibility of the synthesized compound was evaluated via the MTT assay, a widely accepted colorimetric method for assessing cell metabolic activity and viability [1], confirming its safety. Finally, the antineoplastic drug TAEAEAP, employed in cancer treatment, underwent molecular docking studies, interacting with molecules 1BD8 (CDK6 monomeric complex with an inhibitor) [23] and 3NUP (structure of inhibitor P19nk4d) [24].

This study focused on the synthesis, structural analysis, and antibacterial properties of a purple-colored complex, Bis[tris(2-ethylaminoethyl)amine]copper(II)dinitrate ((TAEAEAP) $_2$ Cu(NO $_3$) $_2$). The complex was formed through the reaction between copper nitrate and TAEAEAP in reflux conditions using 97% ethanol as the solvent for 4 hours. The formation of this purple complex occurred over several months in a dark environment and at ambient temperatures. Structural characterization was

performed using analytical techniques such as IR spectroscopy, CHN analysis, and atomic absorption spectroscopy. Furthermore, the antibacterial efficacy of the copper complex against Gram-positive *Staphylococcus aureus* ATCC 6538 (G+), and *Bacillus subtilis* 2a (ATCC 23857 G (+)) was also examined.

Experimental

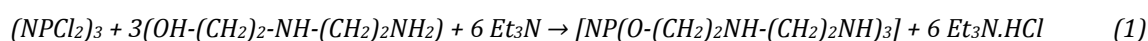
Chemical preparation

In the experimental section, we utilized analytical-grade reagents for all chemicals and solvents. The L929 fibroblast cells were sourced from Pasteur Bank in Tehran. The infrared (IR) spectrum was recorded on a Thermo Nicolet FT-IR spectrometer using KBr tablets within the range of 400-4000 cm^{-1} . UV-Visible (UV-Vis) data were measured using a Shimadzu UV-VIS 2550 spectrophotometer Labomed, INC UVD2950 at ambient temperature, covering a range of 190-1100 nm. For nuclear magnetic resonance (NMR) analysis, a Bruker Avance DPX 250 instrument operating at 2550a MHz was employed to obtain ^1H -NMR, ^{13}C -NMR, and ^{31}P -NMR spectra. Fluorescence measurements were conducted utilizing a PerkinElmer LS45 Fluorescence Spectrometer. In addition, the antibodies and antigens of the infectious agent were detected using an Epoch Eliza reader from Bio-Rad. Elemental analysis of CHN was performed using a Thermo Finning Flash Elemental Analyzer (1112 EA) (Thermo Fisher Scientific Inc., Waltham, MA, USA). The melting point was measured on an electrically heated Barnsted Electrothermal 9200 apparatus. *Staphylococcus aureus* ATCC 6538 (G+), and *Bacillus subtilis* 2a ATCC 23857 (G+) were obtained from the Pasteur Bank, Tehran. In the preparation of the material for this study, the measurement of copper (Cu) content was conducted using the MGA-1000 lumex Atomic Absorption Spectrometer.

Synthesis of (8s,10s,19s)-1,11,20-trioxa-4,7,9,14,17,18,23,26,27-ninaaza-8 χ^5 ,10 χ^5 ,19 χ^5 -triphosphatrispiro[7.1.7 10 .1.7 19 .1 8]heptacosa-8(27),9,18-triene [N $_3$ P $_3$ (OC $_2$ H $_5$ NC $_2$ H $_5$ N) $_3$]

In accordance with Equation 1, a solution was prepared by dissolving 0.3 g (3 mmol) of 2-[(2-aminoethyl)amino]ethanol in 30 mL of anhydrous toluene. Then, 1.3 mL (6 mmol) of triethylamine was added gradually while stirring the amino-alcohol solution on a magnetic stirrer. After approximately 15 minutes, 0.03 g (1 mmol) of $N_3P_3Cl_6$ was added to 25 mL of toluene in the same way. The mixture was heated to 70 °C under anhydrous conditions for 9 days in a round-bottom flask with a glass stopper. The clear liquid separated from the dark yellow oily precipitate. The reaction solution was carefully evaporated using a rotary evaporator to yield a viscous dark yellow oil. Subsequently, this product was dissolved in dichloromethane (DCM) and subjected to two successive

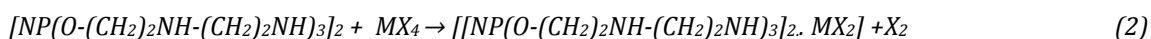
extractions with 10 mL of distilled water each. Through this process, the transfer of triethylamine hydrochloride occurred from the organic phase to the aqueous phase, facilitating its removal from the final product. After evaporation of DCM, pale-yellow oil was obtained. The yield was ~ 0.16 g. (36%). ^{31}P -NMR (DMSO, ppm): δ 0.52 (s, P). 1H -NMR (DMSO, ppm): δ 2.25 (p, 1H, $^5J_{H-H} = 4.4$ Hz, NH); 2.66-2.41 (m, 4H, CH_2 -NH- CH_2 , NH- CH_2), 2.97 (s, 2H OH₂); 3.40 (t, 1H, $^3J_{H-H} = 5.8$ Hz, NH). ^{13}C NMR (DMSO, ppm): δ 43.46-34.33 (m, CH_2 -O), 52.43 (d, $J = 44.2$ Hz, CH_2 -NH); 60.85 (s, CH_2 -NH). FTIR (KBr, cm^{-1}): ν 3442 (NH), 2959, 2860 (C-H), 1598 (NH bend), 1463 (CH bend), 1287, 1123, 958 (P=N), 1072 (C-N), and 742 (NH wag). UV-Vis (DMSO, nm): λ_{max} 295, 345. PL (DMSO, nm): λ_{max} 488.



Synthesis Bis [tris(2-ethylaminoethyl)amine]copper(II)dinitrate
 $[[N_3P_3(OC_2H_5NC_2H_5N)_3]_2Cu(NO_3)_2]$

Based on Equation 2, a dark blue solution was prepared by combining 2 mmol (equivalent to 0.8 g) of the ligand TAEAEAP with 1 mmol (equivalent to 0.24 g) of copper(II) nitrate in 30 cc of 98% ethanol. The mixture was allowed to react at room temperature conditions for 30 minutes, followed by a reflux period of 5 hours at 72 °C. Subsequently, the solution was subjected to filtration and solvent extraction, resulting in the formation of a viscous, blue precipitate at the

bottom of the vessel. Over a period of six months, a small purple mass gradually emerged at the precipitate's base. This material was subsequently purified through washing with methanol and subjected to drying. The paper solid yield was (0.8g). (64%), m.p = 195°. FTIR (KBr, cm^{-1}): ν 3309 (NH), 3254, 3217 (C-H), 1592 (NH bend), 1444 (CH bend), 1407(NO_3), 1107, 1060, 686 (P=N), 1085(C-N), and 980 (NH wag). Anal. Calcd. for $C_{24}H_{60}CuN_{20}O_{12}P_6$: C, 26.93; H, 5.65; N, 26.17; Found: C, 27.43.10; H, 7; and N, 28.2.



Preparation of stock solution of $[N_3P_3(OC_2H_5NC_2H_5N)_3]$ and metal ions

Distilled water was employed to create standard stock solutions of TAEAEAP at a concentration of 1 mM and metal chloride at a concentration of 0.001 M. Subsequently, 0.1 ml of the 1 mM TAEAEAP solution was introduced into a 10 ml volumetric flask, and then diluted with a mixture of distilled water and methanol in a ratio of 9:1. Finally, the TAEAEAP solution was supplemented

with 10 equivalents of metal ion salts to initiate the fluorescence detection process.

Computational methodology

In the experimental section, we employed Gaussian09 [25] and GaussView [26] software to elucidate the structure of the synthesized product in its solid state, optimize its geometry, determine its symmetry, and measure bond lengths and angles. Density functional theory (DFT) structural optimization and frequency

calculations were carried out using the M06-2x functional and the 6-31G basis sets, implemented within the Gaussian package [27].

For the docking procedure, we utilized AutoDock Vina v.1.2.0 in conjunction with Chimera and Discovery Studio. AutoDock Vina, an open-source application for molecular docking, was developed and implemented by Dr. Oleg Trott at The Scripps Research Institute's Molecular Graphics Lab (now CCSC). UCSF Chimera, created by the University of California, San Francisco's Resource for Biocomputing, Visualization, and Informatics (www.rbvi.ucsf.edu/chimera), received funding from the National Institutes of Health (P41-GM103311). BIOVIA[28], BIOVIA 27, developed by Dassault Systems, is a comprehensive molecular modeling application for visualizing, sharing, and analyzing data related to proteins and small molecules. It is integrated into Discovery Studio, San Diego, enabling seamless collaboration among experts and colleagues without the loss of scientific knowledge or time. The structural information for transferase/transferase inhibitor 3NUP (CDK6 monomeric in complex with inhibitor, PDB DOI: 10.2210/pdb3NUP/pdb) and tumor suppressor 1B8D (structure of CDK inhibitor P19INK4D, PDB DOI: 10.2210/pdb1BD8/pdb) was obtained from the Protein Data Bank (<https://www.rcsb.org>).

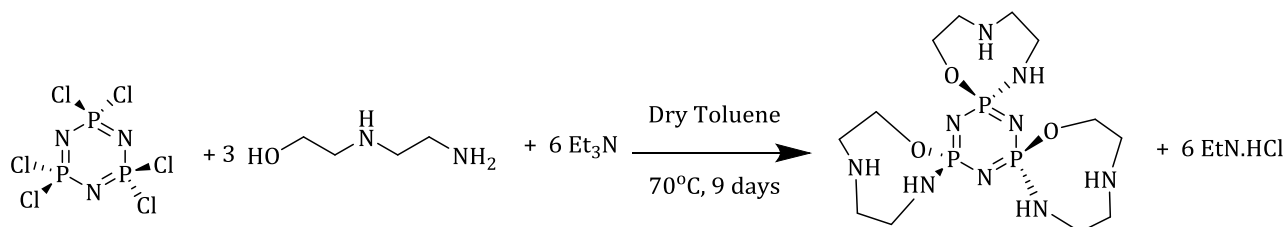
Antibacterial activity

This study aimed to assess the antibacterial efficacy of compound,

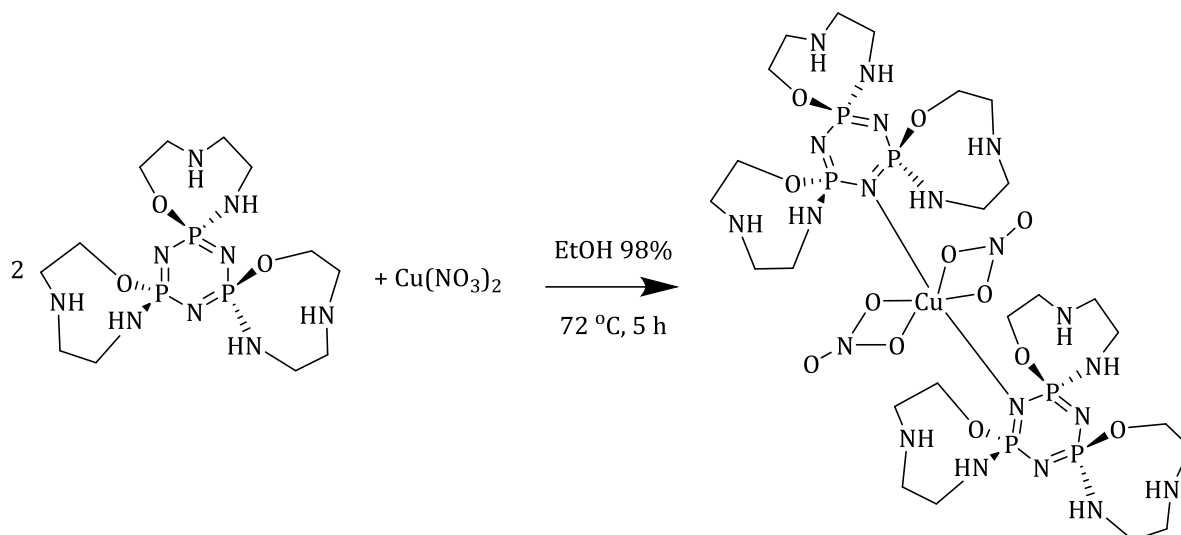
$[[N_3P_3(OC_2H_5NC_2H_5N)_3]_2Cu(NO_3)_2]$ against bacterial strains, specifically *Staphylococcus aureus* ATCC 6538 (G+), and *Staphylococcus aureus* ATCC 6538 (G+). The bacterial strains were sourced from the American Type Culture Collection (ATCC) and cultivated in Luria-Bertani (LB) broth under standardized conditions. The compounds were prepared in various concentrations and tested using the zone-of-inhibition method. Results were quantified by measuring the diameter of the inhibition zones around each compound-impregnated disk, with data analysis performed using Image J software [29]. This research provides valuable insights into the antibacterial potential of compounds III and IV against these two bacterial species.

Results and Discussion

In our synthesis, we successfully synthesized tris-bis(triazaphosphorine ethylenediamine) (TAEAEAP) by cyclizing (HCCTP) in a 1:3 ratio with the bifunctional N/O donor, 2-[(2-aminoethyl)amino]ethanol. This reaction was conducted in an anhydrous toluene environment with triethylamine serving as the hydrogen chloride acceptor. Notably, the cyclization proceeded with spiro-regiospecificity, as illustrated in Scheme 1. The copper complex, tris-bis(triazaphosphorine ethylenediamine)Cuprate (II)-di-nitrate (TAEAEAP)₂Cu(NO₃)₂, was subsequently synthesized in a 1:2 ratio using Cu(NO₃)₂·2H₂O and TAEAEAP in 98% ethanol. The structural representation of the copper complex is presented in Scheme 2.



Scheme 1: Mechanism of TAEAEAP synthesis through the HCCTP cyclization in a 1:3 ratio with 2-(2-aminoethyl) amino ethanol, using dry toluene and triethylamine as the hydrogen chloride acceptor. The cyclization proceeds with spiro-regiospecificity



Scheme 2: The Synthetic mechanism of bis(tris(2-ethylaminoethyl)amine)copper(II)dinitrate. This synthesis is achieved through the reaction of Copper (II) nitrate with TAEAEAP in a 2:1 ratio, specifically in ethanol with a purity of 98%

NMR results

In our analysis, we acquired ^{31}P -NMR, ^1H -NMR, and ^{13}C -NMR spectra of TAEAEAP dissolved in dimethyl sulfoxide (DMSO) at a temperature of 300 °C. The ^{31}P NMR spectrum displayed a singlet signal at $\delta = -0.52$, indicating the coupling between hydrogen and phosphorus in the A3 spin system, as illustrated in Figure 1. These spectra provided conclusive evidence that the compound had been fully substituted by amino alcohol, with all three phosphorus atoms residing in identical chemical environments. The amines within the phosphazene ring substituents manifested as pentets ($\delta = 2.25$, $J = 4.4$ Hz, 1H) and triplets ($\delta = 23.40$, $J = 5.8$ Hz, 1H).

In the ^1H -NMR spectrum, as depicted in Figure 2, it was observed that the compound featured two intermolecular carbon-hydrogen bonds with distances of 2.74 and 2.89 Å, respectively. Furthermore, intramolecular hydrogen bonds involving the oxygen atoms were evident, represented by a singlet peak at 2.79 ppm, as demonstrated in Figure 3. The ^{13}C -NMR spectrum in Figure 4 revealed two distinct signals: a doublet at 33.89 ppm and a multiple in the 46-47 ppm range. These signals strongly suggested the presence of hydrogen bonds formed between the oxygen atoms and the hydrogens attached to the carbons.

Infrared spectroscopy

The IR spectra of the product and the precursors in Figure 5 show the presence of the phosphazene ring by the peak in the region 1287.91, 1123.08 cm^{-1} , which corresponds to the asymmetric stretching vibrations of P=N. The symmetric stretching of P-N gives another peak in the region of 958 cm^{-1} . The OH peak in the product is absent, and the peak in the region of 3442.86 is due to the amino group. The lack of the phosphorus-chlorine signal between 621.33 and 524.42 cm^{-1} indicates that amino alcohols have completely replaced chlorine on phosphorus. [30].

In the analysis of the IR spectrum for the $(\text{TAEAEAP})_2\text{Cu}(\text{NO}_3)_2$ complex, two distinctive absorption bands were observed, both associated with the P=N group, occurring at 1107 cm^{-1} and 1060 cm^{-1} . Notably, these bands appeared at lower wavenumbers when compared to TAEAEAP, indicating structural differences in the complex. Furthermore, a comparison of the ν (NH) vibrational frequency in the copper complex with the free TAEAEAP ligand revealed a notable shift of this vibration by 33 cm^{-1} towards higher frequencies upon complexation. In addition, an absorption band in the 1407 cm^{-1} region was identified, which is attributed to the nitrate group. Detailed information on the IR

absorption bands for the four compounds, namely HCCP, TAEAEAP, (AEAE), and (TAEAEAP)₂Cu(NO₃)₂, is provided in Table 1 for reference.

Table 1 presents the characteristic absorption bands, including P=N group vibrations, ν (NH) vibrational frequencies, and nitrate group-related frequencies, as observed in the IR spectra of the specified compounds.

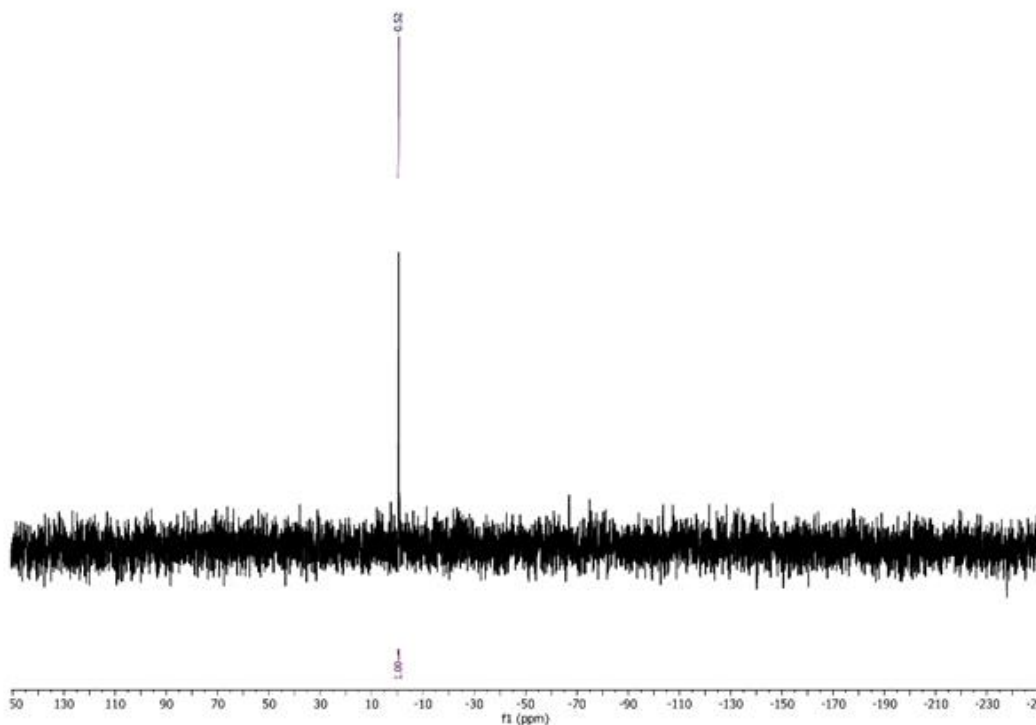


Figure 1: ³¹P NMR spectrum of TAEAEAP

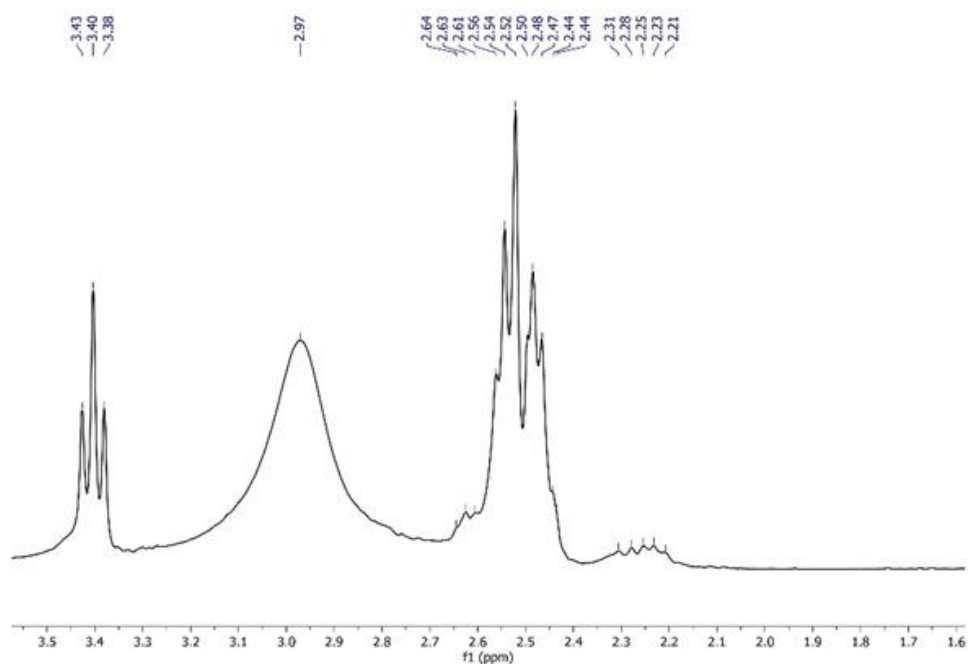


Figure 2: ¹H NMR spectrum of TAEAEAP

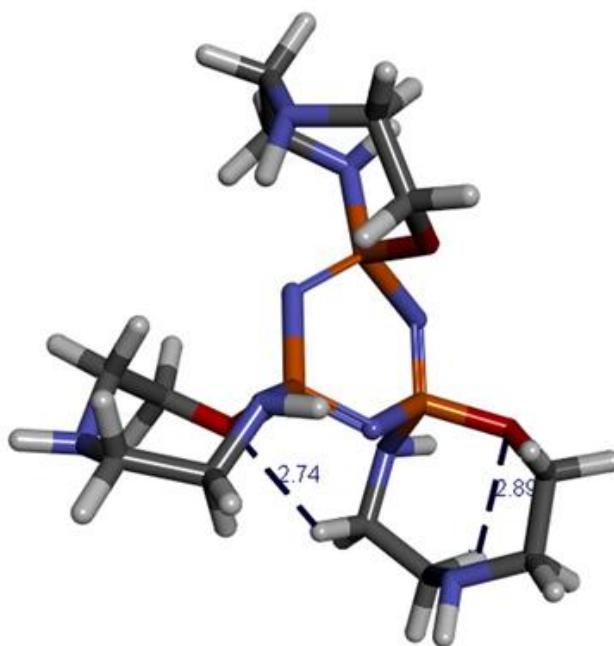


Figure 3: Intra hydrogen bonds in the TAEAEAP structure were calculated with chimera and discovery studio

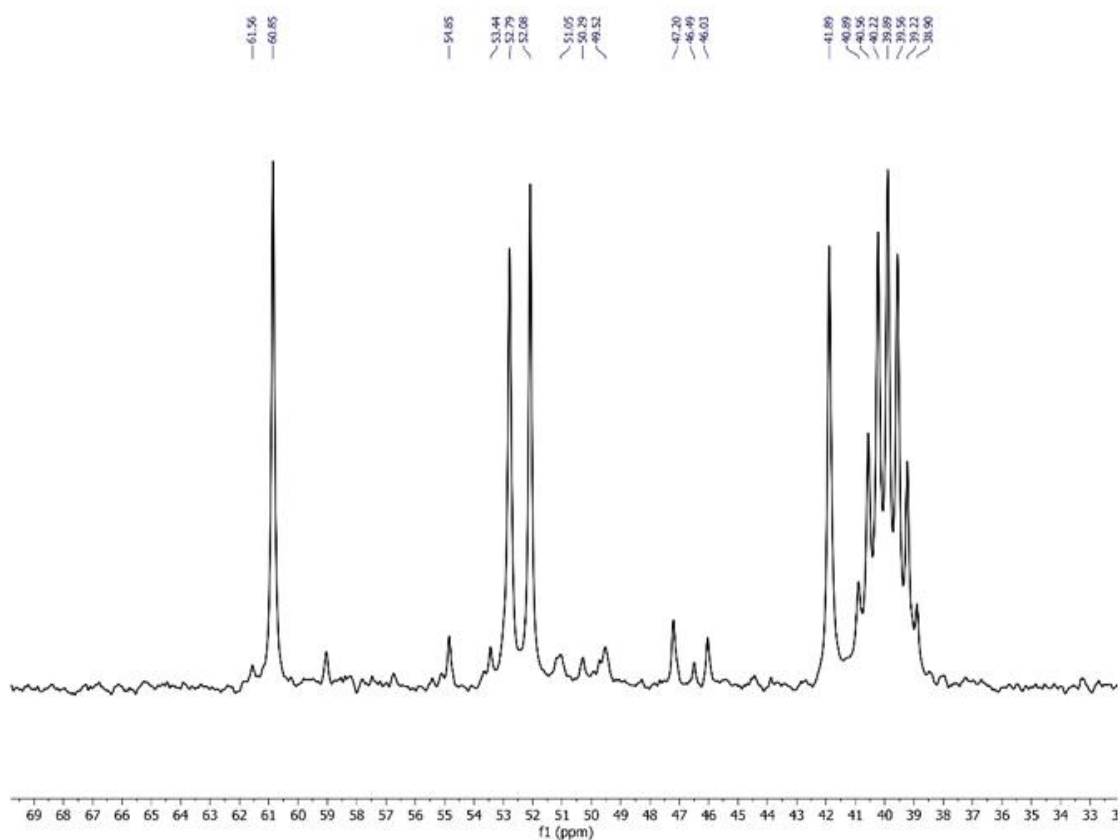


Figure 4: ¹³C-NMR spectrum of TAEAEAP

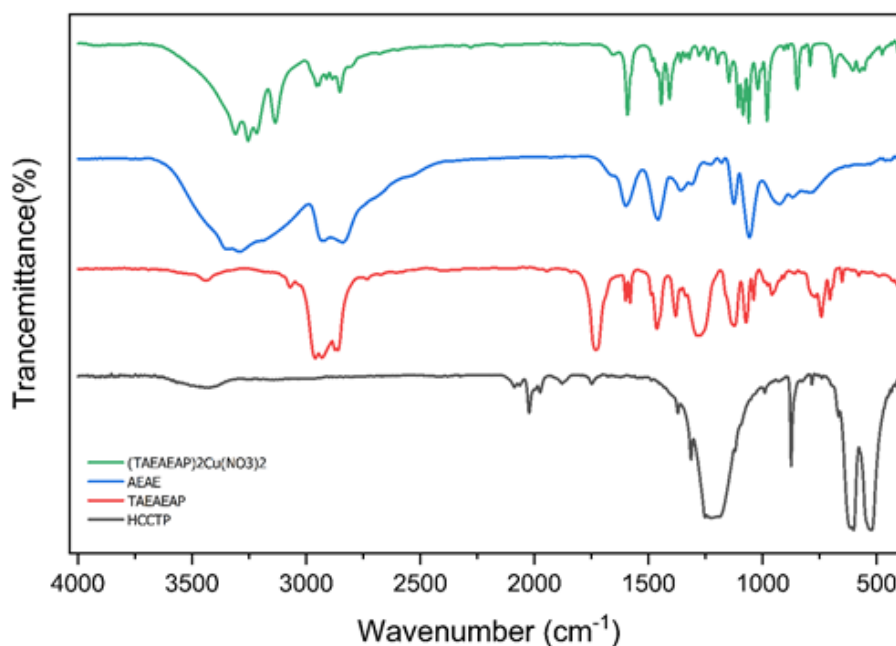


Figure 5: IR spectra of AEAE, TAEAEAP, HCCTP, and $(\text{TAEAEAP})_2\text{Cu}(\text{NO}_3)_2$, respectively

Table 1: Presents the infrared spectroscopic absorption bands for HCCP, TAEAEAP, (AEAE), and $(\text{TAEAEAP})_2\text{Cu}(\text{NO}_3)_2$. Furthermore, it includes a comparison of the absorption intensities to assess the cadence of absorption for the specified compounds

Absorption bands	AEAE	HCCP	TAEAEAP	$(\text{TAEAEAP})_2\text{Cu}(\text{NO}_3)_2$
(ν N-H)	3287 cm^{-1}		3442 cm^{-1}	3309 cm^{-1}
(ν C-H)	2924, 2840 cm^{-1}		2959, 2860 cm^{-1}	3254, 3217 cm^{-1}
(ν_{as} P=N)		1243, 1180 cm^{-1}	1287, 1123 cm^{-1}	1107, 1060 cm^{-1}
(ν C-N)	1057 cm^{-1}		1072 cm^{-1}	1085 cm^{-1}
(ν_{s} P=N)		873 cm^{-1}	958 cm^{-1}	980 cm^{-1}
(NH wag)	796 cm^{-1}		742 cm^{-1}	686 cm^{-1}
(ν O-H)	3354 cm^{-1}			
(ν P-Cl)	622 cm^{-1}	532 cm^{-1}		
(N-H bend)	1598 cm^{-1}		1598 cm^{-1}	1592 cm^{-1}
(ν NO ₃)				1407 cm^{-1}
(C-H bend)	1458 cm^{-1}		1463 cm^{-1}	1444 cm^{-1}

Ultraviolet and fluorescence studies

The UV spectrum of TAEAEAP in DMSO at a concentration of 4×10^{-7} mol/ml and room temperature is depicted in Figure 6. It shows two absorbance bands at 295 nm and 345 nm. The band at 295 nm is related to π - π^* transitions of the phosphazene ring. The replacement of chlorine by 2-[(2-aminoethyl) amino] ethanol on

the phosphazene ring leads to a red shift of P=N, resulting in the band at 295 nm. The band at 345 nm may be attributed to intramolecular charge transfer within the 2-[(2-aminoethyl) amino] ethanol moiety attached to the phosphazene ring [31]. In the UV analysis of the complex, conducted in an aqueous solvent, three distinct absorption bands were observed at wavelengths

of 194.8 nm, 255.6 nm, and 871.6 nm. The 871.6 nm band was attributed to d-d transitions within the complex. Therefore, by changing the solvent polarity from DMSO to water, the absorption bands of TAEAEAP shifted to less visible wavelengths, indicating a change in the electronic transitions occurring within the

molecule. The fluorescence properties of the oily cyclotriphosphazene derivatives were examined in DMSO using diluted solutions at a concentration of 4×10^{-7} mol/ml. A fluorescence band was observed at approximately 488 nm [30] (Figure 7).

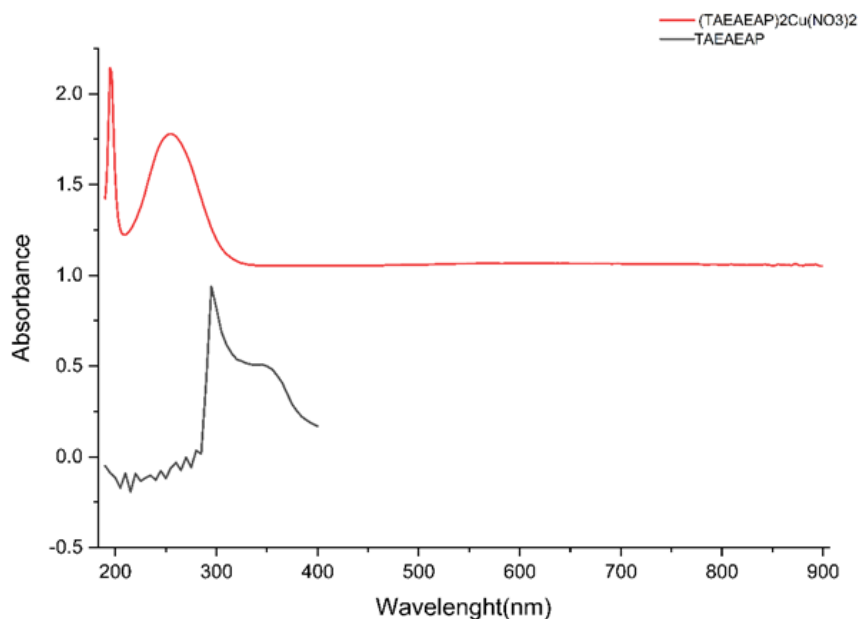


Figure 6: UV Spectrum of TAEAEAP in DMSO at a concentration of 4×10^{-7} mol/ml and UV-Visible Spectra of the complex $(\text{TAEAEAP})_2\text{Cu}(\text{NO}_3)_2$ in aqueous solution at a concentration of 4×10^{-7} mol/m

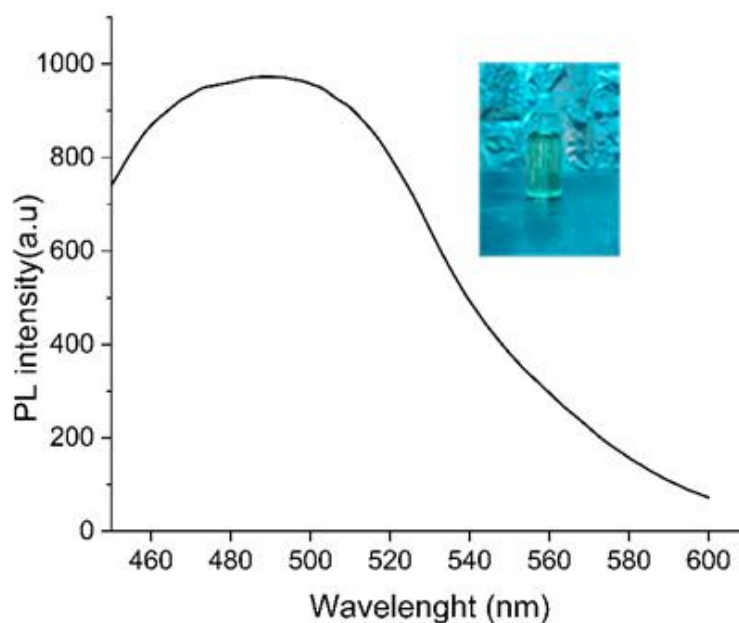


Figure 7: Fluorescence spectrum of compound TAEAEAP (4×10^{-7} M, excited at 400 nm) in DMSO

Atomic absorption

Based on the results obtained from atomic absorption analysis, it is evident that the sample under investigation, which was in powder form, underwent acid dissolution for analysis. The focus of this analysis was on the determination of copper (Cu) content within the sample. The results indicate that the sample contains approximately 20% copper, expressed in terms of elemental percentage. It is important to note that these results are reported without considering the potential effects of the sample matrix. The accuracy and reliability of these findings are contingent on the methodology employed and the sample preparation process.

Computational Studies

The structure obtained from density functional theory (DFT) calculations is demonstrated in

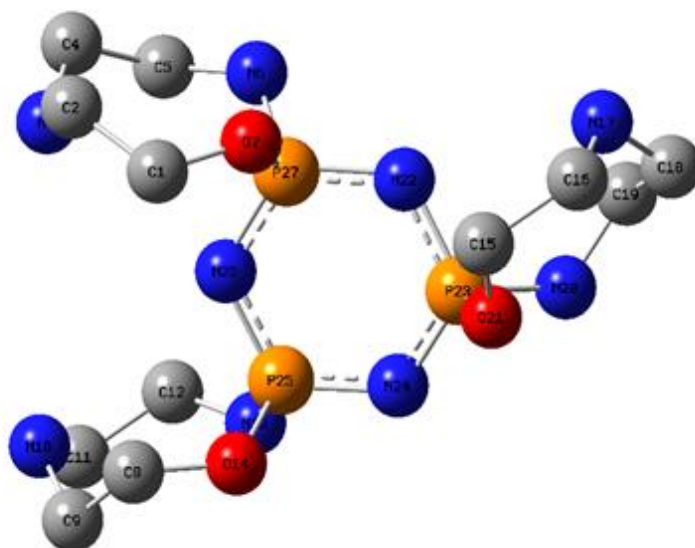
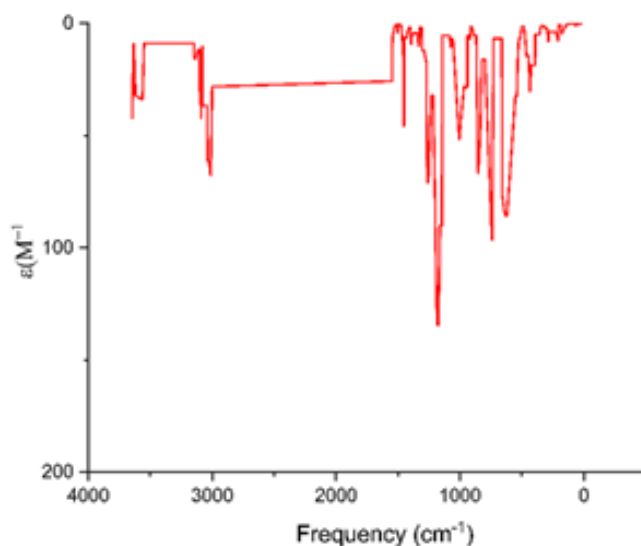
Figure 8. The structure comprised heterocyclic molecules attached to the $N_3P_3Cl_6$ core through distorted 8-membered rings. Due to steric effects, the structure exhibited non-planarity and deviation. It exhibited C_1 symmetry and possessed estimated stability energy of approximately 5821753.473 KJ. Bond lengths and angles between the atoms are presented in **Table 2**. Comparisons were made between the experimental infrared spectrum of TAEAEAP and the calculated infrared spectrum (**Figure 9**). The results from **Figure 9** were summarized in **Table 3**. Upon comparison of **Tables 3** and **1**, it was evident that both spectra were similar, albeit with minor differences in signal intensity. These discrepancies could be attributed to variations in the states of the materials used in the experimental and computational procedures [32].

Table 2: The calculated structural data of TAEAEAP

The bond lengths and angles measurements	
P23-N22	1.61509
N22-P27	1.59751
P27-N26	1.60432
N26-P25	1.60747
P25-N24	1.59353
N24-P23	1.59886
P25-O14	1.62027
P25-N13	1.66126
P23-O21	1.61377
P23-N28	1.66606
P27-O7	1.63111
P27-N6	1.66204
N26-P27-N22	118.47336
N22-P23-N24	116.40654
N26-P25-N24	118.92434
O14-P25-N13	107.20012
O21-P23-N20	103.67251
O7-P27-N6	106.90955

Table 3: Comparative analysis of experimental and calculated infrared spectra for TAEAEAP

Absorption bands	(ν N-H)	(ν C-H)	(ν_{as} P=N)	(ν C-N)	(ν_s P=N)	(N-H bend)	(NH wag)
Calculated TAEAEAP	3564 cm^{-1}	3088, 3012	1264, 1184	1005	851	1548	700

**Figure 8:** The optimized conformation of TAEAEAP (by removing hydrogens) from M06-2x of Gaussian**Figure 9:** Frequency diagram obtained from DFT calculations

Docking studies

We performed a docking study using AutoDock Vina (v1.2.0) [33,34] and Chimera 15.1 for 3NUP (CDK6 monomeric complex with the inhibitor)

and 1BD8. 3NUP is a transferase/transferase inhibitor. Figure 10 shows the best pose with the lowest energy mode of interaction between TAEAEAP and 3NUP. The hydrogen bond length between TAEAEAP and THR267 was

approximately 1.887 Å. Figure 11 shows the lowest energy hydrogen bond when studying the molecular docking between the tumor

suppressor 1BD8 and TAEAEAP. The hydrogen bond distance between TAEAEAP and MET1 was 2.089 Å.

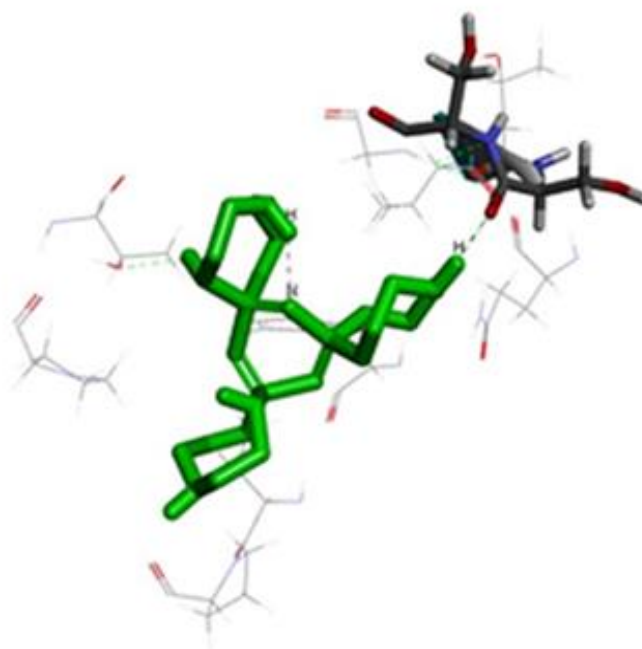
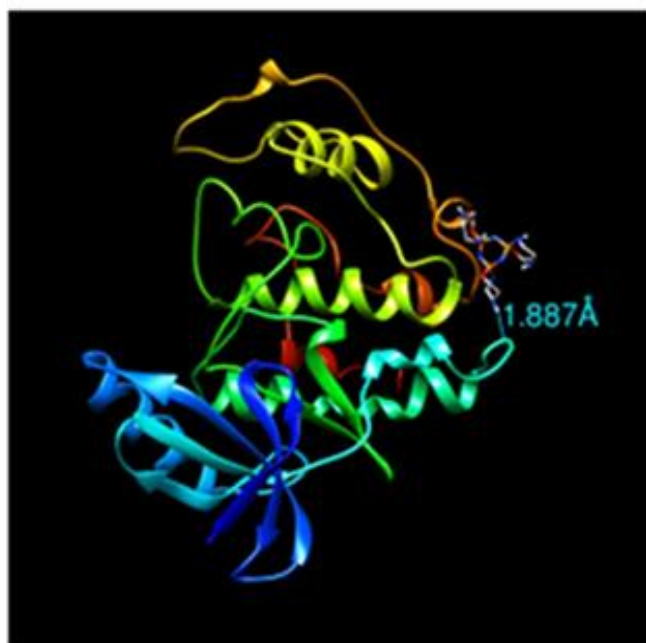


Figure 10: Molecular docking of TAEAEAP with 3NUP

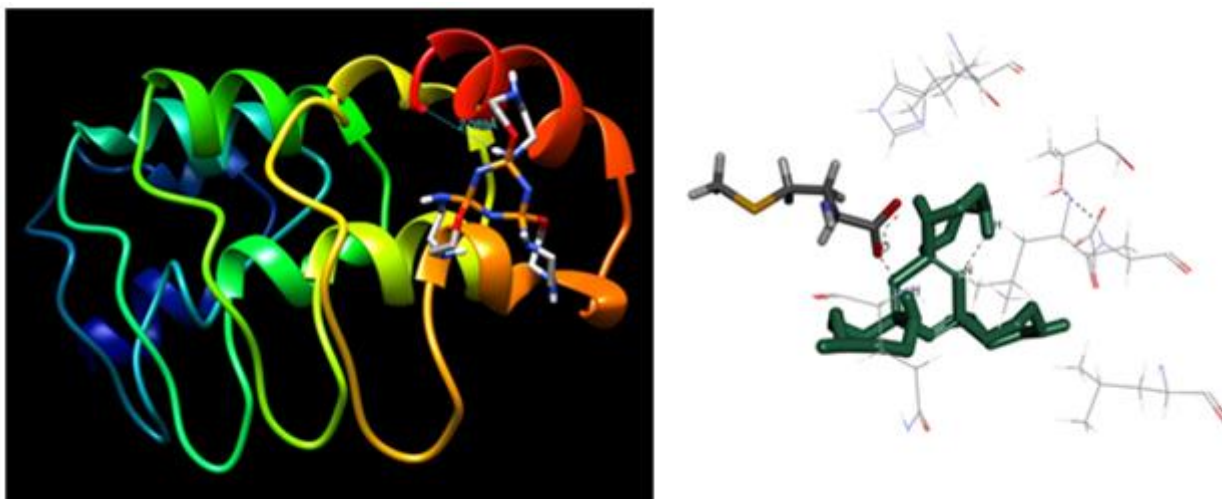


Figure 11: Molecular docking of TAEAEAP with 1BD8

Metallic ion sensing characteristics

The fluorescence emission of TAEAEAP was observed at 432 nm when excited at 400 nm. The phosphazene derivative compound was tested for its chemical sensing properties by adding four metal ions (Pb^{2+} , Cd^{2+} , Cu^{2+} , and Ni^{2+}) to a mixture of (9:1 v/v) H_2O /methanol (Figure 12). The fluorescence emission of TAEAEAP increased with the addition of Cd^{2+} and Pb^{2+} and decreased with the addition of Ni^{2+} and Cu^{2+} .

Cytotoxicity of $[\text{N}_3\text{P}_3(\text{OC}_2\text{H}_5\text{NC}_2\text{H}_5\text{N})_2]$

The biocompatibility of TAEAEAP was thoroughly assessed through cell viability assays employing L929 fibroblast cells. The MTT assay, a widely recognized method for evaluating cytotoxicity, was conducted across a spectrum of TAEAEAP concentrations ranging from 7.8125 to 1000 g/mL. The results, as illustrated in Figure 13, unequivocally demonstrate that TAEAEAP exhibited no significant cytotoxic effects on the L929 fibroblast cells within the tested concentration range. In addition, the WST-1

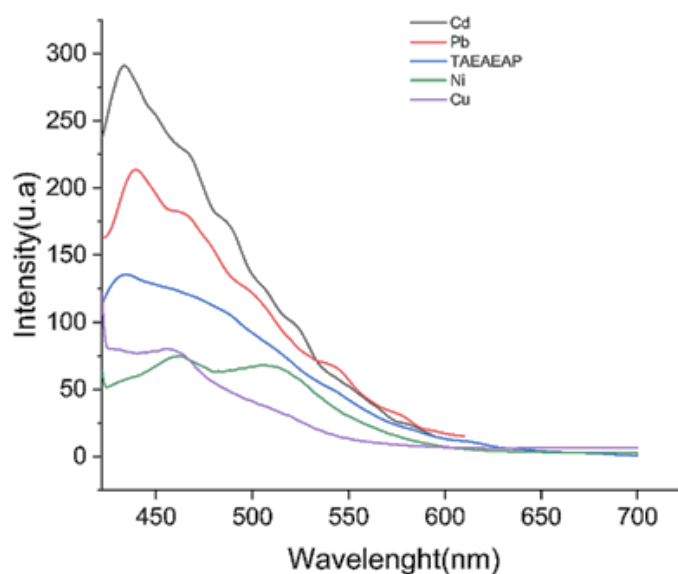


Figure 12: Fluorescence changes of the solution containing TAEAEAP and 10 equiv of addition of Pb^{2+} , Cd^{2+} , Cu^{2+} , and Ni^{2+} in room temperature

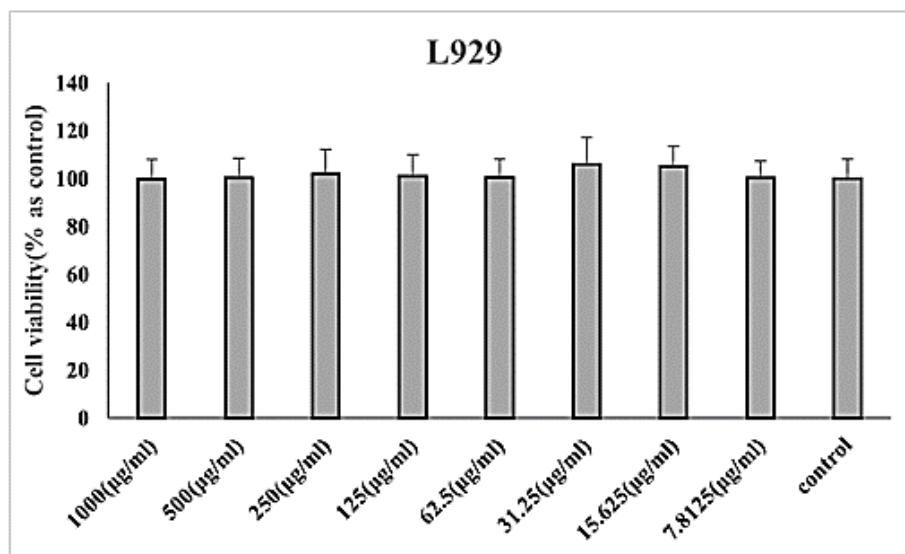


Figure 13: Cytotoxicity effect of TAEAEAP on fibroblast cells

assay further corroborated these findings, affirming the compound's compatibility with healthy cell lines.

In addition to manifesting biological compatibility, as evidenced by the findings elucidated in the cytotoxicity assessment and the subsequent elucidation of metallic ion sensing characteristics in Section 3.7, TAEAEAP exhibits

auspicious attributes in terms of environmental compatibility and chemical sensing properties.

Antibacterial assay

We tested the antibacterial activity of compound $(\text{TAEAEAP})_2\text{Cu}(\text{NO}_3)_2$ against *Staphylococcus aureus* ATCC 6538 (G+), and *Bacillus subtilis* 2a ATCC 23857 G(+) bacteria using the disk diffusion method [35]. Four concentrations (2, 5, 10, and

Table 4: The measurements of inhibition diameters around the disks of antibacterial assay

Diameter of inhibition zone (mm)		
Target strains	Solution concentration (mg/mL)	Zone of inhibition (mm) for Compound $(\text{TAEAEAP})_2\text{Cu}(\text{NO}_3)_2$
<i>Staphylococcus aureus</i> ATCC 6538	2	12.22
	5	13.88
	10	14.35
	20	19.123
<i>Bacillus subtilis</i> 2a ATCC 23857	2	7.14
	5	11.26
	10	14.12
	20	19.83

20 mg/mL) of compound in DMSO were applied to filter paper disks. The disks were placed on agar plates with bacterial strains and incubated

at 37 °C for 24 hours. The zones of inhibition around the disks were measured to determine the effectiveness of the compound (Table 4).

Conclusion

In conclusion, the evaluation of the cytotoxicity of TAEAEAP using L929 fibroblast cells demonstrated no toxicity at the given concentrations. The cytotoxic response of cell lines and the inhibitory effect of the compound on growth were assessed using the MTT assay. The presence of the phosphazene ring in the product and precursors was confirmed by the IR spectra, which exhibited peaks corresponding to the asymmetric and symmetric stretching vibrations of P=N and P-N, respectively. The absence of the OH peak and the presence of the amino group peak further indicated the replacement of chlorine by amino alcohols on phosphorus. The UV spectrum of TAEAEAP exhibited two absorbance bands at 295 nm and 345 nm, attributed to π - π^* transitions of the phosphazene ring and intramolecular charge transfer within the 2-[(2-aminoethyl) amino] ethanol moiety, respectively.

Furthermore, the fluorescence properties of the oily cyclotriphosphazene derivatives were examined, revealing a fluorescence band at approximately 488 nm. Density functional theory (DFT) calculations provided insight into the structure of TAEAEAP, which consisted of heterocyclic molecules attached to the $N_3P_3Cl_6$ core via distorted 8-membered rings. Docking studies using AutoDock Vina and Chimera 15.1 elucidated the interactions between TAEAEAP and the transferase/transferase inhibitor 3NUP, as well as the tumor suppressor 1BD8, highlighting the formation of hydrogen bonds with specific amino acid residues.

We have investigated the synthesis, structure, and antibacterial activity of the $(TAEAEAP)_2Cu(NO_3)_2$ complex, which exhibits a striking purple color. The complex has proven to be a potent antimicrobial agent against the *Staphylococcus aureus* ATCC 6538 and *Bacillus subtilis* 2a ATCC 23857 strains. Our study has established a direct relationship between the concentration of the complex and its ability to inhibit the bacterial growth.

Acknowledgements

We are grateful to Payam Noor University of Iran for laboratory support.

Funding

This research did not receive any specific grant from funding agencies in the public, commercial, or not-for profit sectors.

Conflict of interest

There are no conflicts of interest to disclose.

ORCID

Camelia Gholamrezazadeh

<https://orcid.org/0000-0002-1960-8679>

Mohammad Hakimi

<https://orcid.org/0000-0001-8179-1622>

Mehdi Dadmehr

<https://orcid.org/0000-0002-6016-5988>

References

- [1]. Hakimi M., Mardani Z., Moeini K., Fernandes M.A., Coordination geometries and crystal structures of cadmium (II) complexes with a new amino alcohol (NN'O) ligand, *Journal of Coordination Chemistry*, 2012, **65**:2221 [[Crossref](#)], [[Google Scholar](#)], [[Publisher](#)]
- [2]. Hakimi M., Mardani Z., Moeini K., Minoura M., Raissi H., Synthesis, Characterization and Crystal Structure of a Binuclear Cadmium Iodide Complex with a Multi-N-donor Oxazolidine Ligand, *Zeitschrift für Naturforschung B*, 2011, **66**:1122 [[Crossref](#)], [[Google Scholar](#)], [[Publisher](#)]
- [3]. Bešli S., Coles S.J., Davies D.B., Erkovan A.O., Hursthouse M.B., Kılıç A., Single-, double- and triple-bridged derivatives of cyclotriphosphazenes with an octafluorohexane-1, 6-diol, *Polyhedron*, 2009, **28**:3593 [[Crossref](#)], [[Google Scholar](#)], [[Publisher](#)]
- [4]. Bešli S., Coles S.J., Davies D.B., Kılıç A., Shaw R.A., Bridged cyclophosphazenes resulting from deprotonation reactions of cyclotriphosphazenes bearing a P-NH group, *Dalton Transactions*, 2011, **40**:5307 [[Crossref](#)], [[Google Scholar](#)], [[Publisher](#)]
- [5]. Ture S., Phosphorus-nitrogen compounds: Reinvestigation of the reactions of hexachlorocyclotriphosphazene with 1, 4-butane- and 1, 6-hexane-diols—NMR studies of the

- products, *Phosphorus, Sulfur, and Silicon and the Related Elements*, 2016, **191**:1174 [[Crossref](#)], [[Google Scholar](#)], [[Publisher](#)]
- [6]. Shaw R.A., The reactions of phosphazenes with difunctional and polyfunctional nucleophilic reagents, *Phosphorus, Sulfur, and Silicon and the Related Elements*, 1989, **45**:103 [[Crossref](#)], [[Google Scholar](#)], [[Publisher](#)]
- [7]. Bešli S., Coles S.J., Davarcı D., Davies D.B., Yuksel F., Effect of chain length on the formation of intramolecular and intermolecular products: Reaction of diols with cyclotriphosphazene, *Polyhedron*, 2011, **30**:329 [[Crossref](#)], [[Google Scholar](#)], [[Publisher](#)]
- [8]. Bešli S., Coles S.J., Davies D.B., Eaton R.J., Kılıç A., Shaw R.A., Competitive formation of spiro and ansa derivatives in the reactions of tetrafluorobutane-1, 4-diol with hexachlorocyclotriphosphazene: A comparison with butane-1, 4-diol, *Polyhedron*, 2006, **25**:963 [[Crossref](#)], [[Google Scholar](#)], [[Publisher](#)]
- [9]. İter E.E., Asmafiliz N., Kılıç Z., Işıklan M., Hoেকেক T., Caylak N., Şahin E., Phosphorus–nitrogen compounds. 14. synthesis, stereogenism, and structural investigations of novel N/O spirocyclic phosphazene derivatives, *Inorganic Chemistry*, 2007, **46**:9931 [[Crossref](#)], [[Google Scholar](#)], [[Publisher](#)]
- [10]. Cho S.Y., Allcock H.R., Dendrimers Derived from Polyphosphazene– Poly (propyleneimine) Systems: Encapsulation and Triggered Release of Hydrophobic Guest Molecules, *Macromolecules*, 2007, **40**:3115 [[Crossref](#)], [[Google Scholar](#)], [[Publisher](#)]
- [11]. Davidson R.J. *Cyclo- and polyphosphazenes grafted with tridentate ligands coordinated to iron (II) and ruthenium (II): a thesis presented in partial fulfilment of the requirements for the degree of Doctor of Philosophy in Chemistry at Massey University, Palmerston North, Massey University*, 2011 [[Google Scholar](#)], [[Publisher](#)]
- [12]. Tao K., Li J., Xu L., Zhao X., Xue L., Fan X., Yan Q., A novel phosphazene cyclomatrix network polymer: Design, synthesis and application in flame retardant polylactide, *Polymer Degradation and Stability*, 2011, **96**:1248 [[Crossref](#)], [[Google Scholar](#)], [[Publisher](#)]
- [13]. Tarassoli A., Nekoeishahraki B., Synthesis of new derivatives of cyclotriphosphazene substituted with the salen side groups, *Journal of the Iranian Chemical Society*, 2011, **8**:1014 [[Crossref](#)], [[Google Scholar](#)], [[Publisher](#)]
- [14]. Jiang P., Gu X., Zhang S., Sun J., Wu S., Zhao Q., Syntheses and characterization of four phosphaphenanthrene and phosphazene-based flame retardants, *Phosphorus, Sulfur, and Silicon and the Related Elements*, 2014, **189**:1811 [[Crossref](#)], [[Google Scholar](#)], [[Publisher](#)]
- [15]. Han R., Ren X.l., Zhang D., Wang M., Yang J.l., Ye Y., Zhao Y., Synthesis and Characterization of Bidentate Cyclotriphosphazene Derivatives, *Phosphorus, Sulfur, and Silicon and the Related Elements*, 2011, **186**:2202 [[Crossref](#)], [[Google Scholar](#)], [[Publisher](#)]
- [16]. Çiftçi G.Y., Eker Y., Şenkuytu E., Yuksel F., Structural and fluorescence properties of the 2, 2'-methylenediphenoxy and 1,1'-methylenedi-2-naphthoxy cyclotriphosphazene derivatives, *Journal of Molecular Structure*, 2016, **1117**:164 [[Crossref](#)], [[Google Scholar](#)], [[Publisher](#)]
- [17]. Itaya T., Honda T., Kusumoto N., Matsumoto A., Inoue K., Fluorescence behavior of water-soluble copolymers with pendant (4-carboxylatophenoxy)cyclotriphosphazene/europium ion complexes, *Polymer*, 2003, **44**:2927 [[Crossref](#)], [[Google Scholar](#)], [[Publisher](#)]
- [18]. Rao M.R., Bolligarla R., Butcher R.J., Ravikanth M., Hexa boron-dipyrromethene cyclotriphosphazenes: synthesis, crystal structure, and photophysical properties, *Inorganic Chemistry*, 2010, **49**:10606 [[Crossref](#)], [[Google Scholar](#)], [[Publisher](#)]
- [19]. Şeker M.G., Akbal T., Atilla D., Avşar N., İbişoğlu H., Synthesis and antimicrobial effects of cyclotriphosphazenes containing monocarbonyl curcumin analogs, *Marmara Pharmaceutical Journal*, 2018, **22** [[Crossref](#)], [[Google Scholar](#)], [[Publisher](#)]
- [20]. Okumuş A., Akbaş H., Kılıç Z., Yasemin Koç L., Açık L., Aydın B., Türk M., Höকেক T., Dal H., Phosphorus–nitrogen compounds part 33: in vitro cytotoxic and antimicrobial activities, DNA interactions, syntheses, and structural investigations of new mono (4-nitrobenzyl) spirocyclotriphosphazenes, *Research on Chemical*

- Intermediates*, 2016, **42**:4221 [[Crossref](#)], [[Google Scholar](#)], [[Publisher](#)]
- [21]. Işıklan M., Asmafiliz N., Ozalp E.E., Ilter E.E., Kılıç Z., Çoşut B.n., Yesilot S., Kılıç A., Öztürk A., Hokelek T., Phosphorus– nitrogen compounds. 21. syntheses, structural investigations, biological activities, and DNA interactions of new N/O spirocyclic phosphazene derivatives. The NMR behaviors of chiral phosphazenes with stereogenic centers upon the addition of chiral solvating agents, *Inorganic Chemistry*, 2010, **49**:7057 [[Crossref](#)], [[Google Scholar](#)], [[Publisher](#)]
- [22]. Dagdag O., Bachiri A.E., Hamed O., Haldhar R., Verma C., Ebenso E., Gouri M.E., Dendrimeric epoxy resins based on hexachlorocyclotriphosphazene as a reactive flame retardant polymeric materials: A review, *Journal of Inorganic and Organometallic Polymers and Materials*, 2021, **31**:3240 [[Crossref](#)], [[Google Scholar](#)], [[Publisher](#)]
- [23]. Velcich A., Klampher L., Maraiadason J., Smartt H., Guilmeau S., Genetics and epigenetics in cancer biology, *Nutritional Oncology*, 2006, **2**:25 [[Google Scholar](#)], [[Publisher](#)]
- [24]. Baumgartner R., Fernandez-Catalan C., Winoto A., Huber R., Engh R.A., Holak T.A., Structure of human cyclin-dependent kinase inhibitor p19INK4d: comparison to known ankyrin-repeat-containing structures and implications for the dysfunction of tumor suppressor p16INK4a, *Structure*, 1998, **6**:1279 [[Google Scholar](#)]
- [25]. M. J. Frisch, G. W. Trucks, H. B. Schlegel, G. E. Scuseria, M. A. Robb, J. R. Cheeseman, G. Scalmani, V. Barone, B. Mennucci, G. A. Petersson, H. Nakatsuji, M. Caricato, X. Li, H. P. Hratchian, A. F. Izmaylov, J. Bloino, G. Zheng, J. L. Sonnenberg, M. Hada, M. Ehara, K. Toyota, R. Fukuda, J. Hasegawa, M. Ishida, T. Nakajima, Y. Honda, O. Kitao, H. Nakai, T. Vreven, J. A. Montgomery, Jr., J. E. Peralta, F. Ogliaro, M. Bearpark, J. J. Heyd, E. Brothers, K. N. Kudin, V. N. Staroverov, R. Kobayashi, J. Normand, K. Raghavachari, A. Rendell, J. C. Burant, S. S. Iyengar, J. Tomasi, M. Cossi, N. Rega, J. M. Millam, M. Klene, J. E. Knox, J. B. Cross, V. Bakken, C. Adamo, J. Jaramillo, R. Gomperts, R. E. Stratmann, O. Yazyev, A. J. Austin, R. Cammi, C. Pomelli, J. W. Ochterski, R. L. Martin, K. Morokuma, V. G. Zakrzewski, G. A. Voth, P. Salvador, J. J. Dannenberg, S. Dapprich, A. D. Daniels, Ö. Farkas, J. B. Foresman, J. V. Ortiz, J. Cioslowski, and D. J. Fox, Gaussian 09 (Gaussian, Inc., Wallingford CT, 2009) [[Publisher](#)]
- [26]. a) Dennington R., Keith T., Millam J., GaussView V., Semichem Inc. *Shawnee Mission KS, GaussView, Version*, 2009, **5** [[Google Scholar](#)] b) Iorhuna F., Ayuba A. M., Nyijime T. A., Muhammedjamiu H., A DTF and Molecular thermodynamic Simulation on the Adsorption Inhibition of Cytarabine a Nucleotides as a Potential Inhibitor on the Aluminium Metal Surface, *Eurasian Journal of Science and Technology*, 2023, **3**:217 [[Crossref](#)], [[Publisher](#)] c) Hoque M., Kumer A., Hussen M. S., Khan M. W., Theoretical Evaluation of 5, 6-Diaroylisoindoline-1,3-dione as Potential Carcinogenic Kinase PAK1 Inhibitor: DFT Calculation, Molecular Docking Study and ADMET Prediction, *International Journal of Advanced Biological and Biomedical Research*, 2021, **9**:77 [[Crossref](#)], [[Publisher](#)] d) Farhami N., A Computational Study of Thiophene Adsorption on Boron Nitride Nanotube, *Journal of Applied Organometallic Chemistry*, 2022, **2**:148 [[Crossref](#)], [[Publisher](#)]
- [27]. Jafari G., Raissi H., Shahabi M., Assessment of sulfobutylether-beta-cyclodextrin as a promising Fluorometholone molecule container: DFT, Docking, Molecular dynamics and MM-PBSA free energy calculations, *Molecular Simulation*, 2022, **48**:168 [[Crossref](#)], [[Google Scholar](#)], [[Publisher](#)]
- [28]. Biovia D.S., BIOVIA discovery studio visualizer, *Software Version*, 2017, **20**:779 [[Google Scholar](#)], [[Publisher](#)]
- [29]. Schneider C.A., Rasband W.S., Eliceiri K.W., NIH Image to ImageJ: 25 years of image analysis, *Nature Methods*, 2012, **9**:671 [[Crossref](#)], [[Google Scholar](#)], [[Publisher](#)]
- [30]. Asmafiliz N., Kılıç, Z., Civan, M., Avcı, O., Gönder, L.Y., Açık, L., Aydın, B., Türk, M., Hökelek, T., Phosphorus–nitrogen compounds. Part 36. Syntheses, Langmuir–Blodgett thin films and biological activities of spiro-bino-spiro trimeric phosphazenes, *New Journal of Chemistry*, 2016, **40**:9609 [[Crossref](#)], [[Google Scholar](#)], [[Publisher](#)]
- [31]. Singh R.K., Kukrety A., Saxena R.C., Chouhan A., Jain S.L., Ray S.S., Phosphazene-based novel

organo-inorganic hybrid salt: synthesis, characterization and performance evaluation as multifunctional additive in polyol, *RSC Advances*, 2017, **7**:13390 [Crossref], [Google Scholar], [Publisher]

[32]. a) Davidson R.J., Ainscough E.W., Brodie A.M., Harrison J.A., Waterland M.R., The nature of the phosphazene nitrogen-metal bond: DFT calculations on 2-(Pyridyloxy)cyclophosphazene complexes, *Europrean Journal of Inorganic Chemistry (Wiley Online Library)*, 2010, 1619 [Crossref], [Google Scholar], [Publisher] b) Iorhuna F., Ayuba A., Nyijime A., Hussain M., Ibrahim M., Comparative Study of Halogen Substituted Isocyanatophosphine as an Adsorptive Inhibitor on Al (110) Crystal Surface, using Density Functional Theory, *Progress in Chemical and Biochemical Research*, 2023, **6**:211 [Crossref], [Publisher] c) Ghasem G., Ramazani A., Zeinali Nasrabadi F., Ahankar H., Ślepokura K., Lis T., Kazami Babaheydari A., Single crystal X-ray structure analysis and DFT studies of 3-hydroxyl-1,7,7-trimethyl-3-[5-(4-methylphenyl)-1,3,4-

oxadiazol-2-yl]bicycle [2.2.1]heptan-2-one, *Journal of Medicinal and Pharmaceutical Chemistry Research*, 2022, **4**:759 [Publisher]

[33]. Eberhardt J., Santos-Martins D., Tillack A.F., Forli S., AutoDock Vina 1.2. 0: New docking methods, expanded force field, and python bindings, *Journal of Chemical Information and Modeling*, 2021, **61**:3891 [Crossref], [Google Scholar], [Publisher]

[34]. Eberhardt J., Santos-Martins D., Tillack, A.F., Forli, S., AutoDock Vina 1.2. 0: New docking methods, expanded force field, and python bindings. *Journal of Chemical Information and Modeling*, 2021, **61**:3891 [Crossref], [Google Scholar], [Publisher]

[35]. Mendez-Vilas A., Science And Technology Against Microbial Pathogens: Research, Development And Evaluation-Proceedings Of The International Conference On Antimicrobial Research (Icar2010), *World Scientific*, 2011, [Google Scholar], [Publisher]

HOW TO CITE THIS ARTICLE

Camelia Gholamrezazadeh, Mohammad Hakimi*, Mehdi Dadmehr. A New and Safe Spirocyclic Alkoxy Phosphazene: Synthesis, Characterization, DFT, Molecular Docking and Photophysical Properties. *Chem. Methodol.*, 2023, 7(12) 944-963.

DOI: <https://doi.org/10.48309/chemm.2023.422145.1735>

URL: https://www.chemmethod.com/article_183865.html